interference terms to the polarization at 90° was found in this way to be $\lesssim 0.3\%$. If only $E1$ and $M1$ amplitudes need be considered then the differential photoneutron polarization [the differential cross section $\sigma(\theta) \times$ the polarization $p(\theta)$] can be written as

$$\sigma(\theta)p(\theta) = A_{EM}\sin\theta + B_{EE,MM}\sin\theta\cos\theta,$$

where A_{EM} depends on $E1$-$M1$ interference and $B_{EE,MM}$ depends on the products of $E1$ and $M1$ amplitudes that lead to different final states of the np system. Of course, only A_{EM} contributes to the polarization at 90°. The primary effect of the MEC is to increase[4] the $M1$ transition amplitudes, namely the $({}^3S_1 + {}^3D_1) \rightarrow {}^1S_0$ transition. Thus, the magnitude of the photoneutron polarization $p(90°)$ must become larger. In order to explain the present data, one must reduce the $M1$ transition amplitude in such a manner that the thermal n-p capture cross section is not changed, or increase the $E1$ transition amplitude in a way that does not alter the total photoabsorption cross section.[13]

Clearly, a high-accuracy angular distribution of photoneutron polarization and cross section is necessary in order to unravel the multipole components of the reaction $^2\mathrm{H}(\gamma,n)\mathrm{H}$ at low energy. In addition, further theoretical work will be necessary in order to explain this simplest nuclear reaction.

We wish to thank B. Day, F. Coester, and E. Hadjimichael for illuminating discussions. This work was supported by the U. S. Department of Energy, Office of Basic Energy Sciences, under Contract No. W-31-109-Eng-38.

[1]E. Hadjimichael, Phys. Lett. 46B, 147 (1973).
[2]H. Arenhovel, W. Fabian, and H. G. Miller, Phys. Lett. 52B, 303 (1974).
[3]M. L. Rustgi, W. Zernik, G. Breit, and D. J. Andrews, Phys. Rev. 120, 1881 (1960).
[4]D. O. Riska and G. E. Brown, Phys. Lett. 38B, 193 (1972).
[5]A. E. Cox, S. A. R. Wynchank, and C. H. Collie, Nucl. Phys. 74, 497 (1965).
[6]M. Bernheim, E. Jans, J. Mougey, D. Royer, D. Tanowski, S. Turck-Chieze, I. Sick, G. P. Capitani, E. De Sanctis, and S. Frullani, Phys. Rev. Lett. 46, 402 (1981).
[7]W. Bertozzi, P. T. Demos, S. Kowalski, C. P. Sargent, W. Turchinetz, R. Fullwood, and J. Russell, Phys. Rev. Lett. 10, 106 (1963).
[8]R. Nath, F. W. K. Firk, and H. L. Schultz, Nucl. Phys. A194, 49 (1972).
[9]L. J. Drooks, Ph.D. thesis, Yale University, 1976 (unpublished).
[10]F. Partovi, Ann. Phys. (N.Y.) 27, 79 (1964).
[11]R. J. Holt, J. R. Specht, H. E. Jackson, and R. M. Laszewski, Nucl. Instrum. Methods 141, 125 (1977).
[12]R. J. Holt, F. W. K. Firk, R. Nath, and H. L. Schultz, Nucl. Phys. A213, 147 (1973).
[13]E. Hadjimichael and D. P. Saylor, Phys. Rev. Lett. 45, 1776 (1980).

High Rydberg States of an Atom in a Strong Magnetic Field

J. B. Delos[a] and S. K. Knudson[b]
College of William and Mary, Williamsburg, Virginia 23185

and

D. W. Noid
Oak Ridge National Laboratory, Oak Ridge, Tennessee 37830

(Received 5 November 1982)

Classical trajectories and semiclassical eigenvalues are calculated for an atomic Rydberg state in a magnetic field. Perturbation theory describes a classical trajectory as a Kepler ellipse which rocks, tilts, and flips in space as orbital parameters evolve slowly in time. Exact numerical calculations verify the accuracy of perturbation theory for $n \simeq 30$, $B \leq 6$ T. Action variables are calculated from perturbation theory and from exact trajectories, and semiclassical eigenvalues obtained by quantization of the action. Good agreement is found with observations.

PACS numbers: 31.20.Wb

The behavior of a highly excited atom in a strong magnetic field is a topic of much current interest.[1] The present studies were motivated by the desire to understand and interpret experimental measurements[2] made at Masschusetts Institute of Technology on one-electron atoms in

TABLE I. Action-angle variables for Kepler orbits.

$I_1 \equiv L_z$	z component of orbital angular momentum
$I_2 \equiv L$	magnitude of orbital angular momentum, $I_2 \geq \lvert I_1 \rvert$
$I_3 = (\mu k^2/-2H_0)^{1/2}$	principal action, related to the Kepler energy, and corresponding to the principal quantum number; $I_3 > I_2$
φ_1	longitude of ascending node (angle in the x-y plane between x axis and line of nodes)
φ_2	argument of perihelion (angle in the plane of the orbit between line of nodes and Laplace vector, which points to perihelion)
φ_3	mean anomaly, related to the true anomaly χ, which is the angle (in the plane of the orbit) between Laplace vector and instantaneous position of particle

states around $n \sim 30$ in magnetic fields of 1–6 T. For such systems the term proportional to B^2 in the Hamiltonian is significant, but still relatively weak, and its effects can be calculated by perturbation theory. We have calculated electron trajectories (for combined Lorentz and Coulomb fields) both by exact numerical methods and by using a form of classical perturbation theory that was developed in celestial mechanics for calculating planetary orbits. Semiclassical energy levels have been obtained by using Bohr-Sommerfeld quantization of action variables.

Consider an atom in a constant magnetic field directed along the z axis. In a frame of reference that is precessing about the z axis at the Larmor frequency, the Hamiltonian for the electron is

$$H = p^2/2\mu - k/r + \lambda(x^2+y^2) = H_0 + \lambda H_1, \tag{1}$$

where $\lambda = e^2B^2/8\mu c^2$ and $k = Ze^2$. With use of classical perturbation theory (as given, for example, in Goldstein[3]) the trajectory of the electron may be described as a Kepler ellipse with orbital parameters that evolve slowly in time. For this purpose, Kepler action and angle variables[3] provide the simplest canonical momenta and coordinates. These are defined in Table I and Fig. 1.

Equations of motion are obtained by rewriting the Hamiltonian (1) in terms of action and angle variables and averaging the canonical equations over one cycle, τ, of the unperturbed Kepler motion:

$$\frac{\Delta\varphi_j}{\tau} = \tau^{-1}\int_0^\tau \left(\frac{\partial H}{\partial I_j}\right)dt = \frac{\partial}{\partial I_j}\left(\frac{\lambda}{\tau}\int_0^\tau H_1 dt\right), \quad j=1,2;$$
$$\frac{\Delta I_j}{\tau} = -\tau^{-1}\int_0^\tau \left(\frac{\partial H}{\partial \varphi_j}\right)dt = -\frac{\partial}{\partial \varphi_j}\left(\frac{\lambda}{\tau}\int_0^\tau H_1 dt\right), \quad j=1,2,3. \tag{2}$$

The average development in time of I_1, I_2, I_3, φ_1, and φ_2 is therefore given by canonical equations

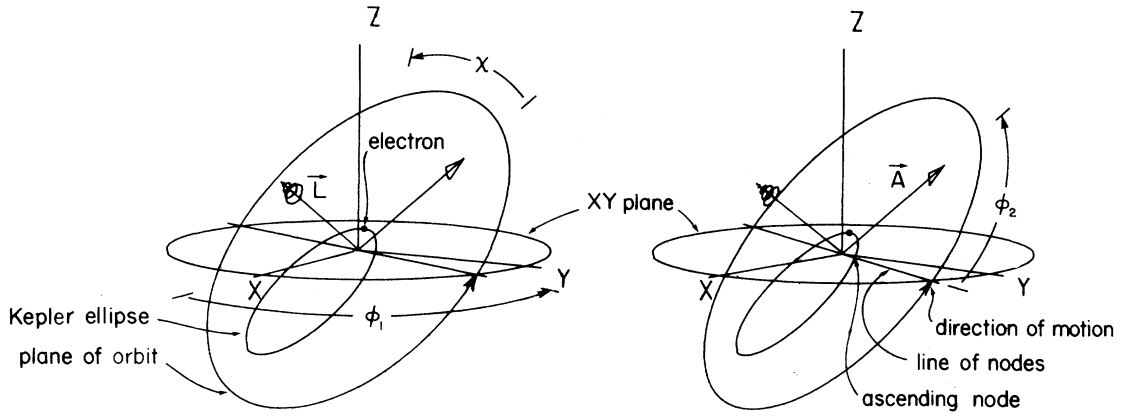

FIG. 1. A Kepler orbit in space. The orbital plane intersects the x-y plane in the line of nodes. The angular momentum vector, $\vec{L}$, with a conical arrowhead, is perpendicular to the orbital plane. The Laplace–Runge–Lenz vector $\vec{A}$ lies in the orbital plane and passes through the perihelion of the Kepler ellipse.

having the effective Hamiltonian

$$\lambda\bar{H}_1(I_2, \varphi_2;\ I_1, I_3) = (\lambda/\tau)\int_0^\tau H_1\, dt. \tag{3}$$

This effective Hamiltonian can be evaluated by a long but straightforward calculation; it turns out to be

$$\lambda\bar{H}_1 = (\lambda/\mu^2k^2)(I_3^2/4I_2^2)[(I_1^2+I_2^2)(5I_3^2-3I_2^2)+5(I_3^2-3I_2^2)(I_2^2-I_1^2)\cos 2\varphi_2]. \tag{4}$$

The behavior of the orbit can be deduced from conservation laws associated with the effective Hamiltonian. L_z and H are of course exact constants of the motion. In addition, since $\lambda\bar{H}_1$ is independent of φ_3, it follows that I_3 is, to first order, a constant of the motion. Now I_3 is related to H_0, which in turn is related to the major axis and the period of the Kepler ellipse, so that it follows that the ellipse evolves under the perturbation in such a way that its major axis, and its zero-order energy, and the period of motion of the particle around the ellipse, do not change with time. In their measurements of the spectrum of high Rydberg states of an atom in a magnetic field, Kleppner and his collaborators[2] found evidence that there may be three conserved quantities associated with the electron motion. In first-order perturbation theory, these conserved quantities are found to be L_z, H, and H_0.

Conservation of H and H_0 implies conservation of $\bar{H}_1$, and this gives further information about the orbit: Since I_1 and I_3 are fixed, I_2 and φ_2 evolve such that the system follows a curve of constant $\bar{H}_1$. A contour plot of $\bar{H}_1(I_2, \varphi_2)$ is shown in Fig. 2. Two types of motion can be seen: clockwise motion around closed loops ("libration") and motion along open contours ("rotation"). A U-shaped separatrix separates rotational and librational curves, and a point of stable equilibrium exists near the center.

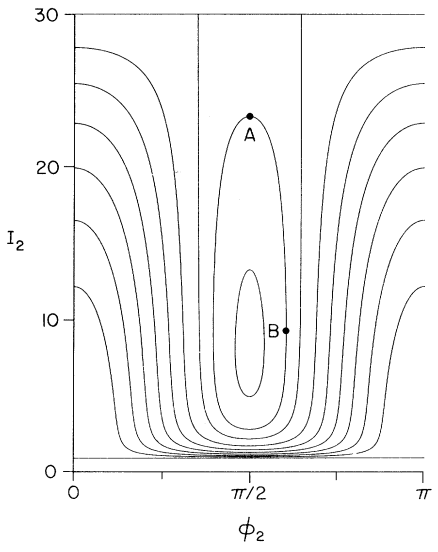

FIG. 2. Contours of constant $\bar{H}_1(I_2, \varphi_2; I_1 = \hbar, I_3 = 30\hbar)$.

With simple reasoning it is now possible to describe the time development of the orbit in space under the influence of the magnetic field. For example, consider motion on a librating trajectory from A to B in Fig. 2. At A $\varphi_2 = \pi/2$, and the Laplace (or Runge-Lenz) vector, which points toward the perihelion of the ellipse, is perpendicular to the line of nodes and lies close to the positive z axis. When φ_2 increases, the Laplace vector tips slightly away from the vertical, and then as $I_2 = |L|$ decreases, the eccentricity of the orbit increases (the minor axis shrinks). Meanwhile, the ignored coordinate φ_1 is increasing, and the plane of the orbit precesses. Similar rea-

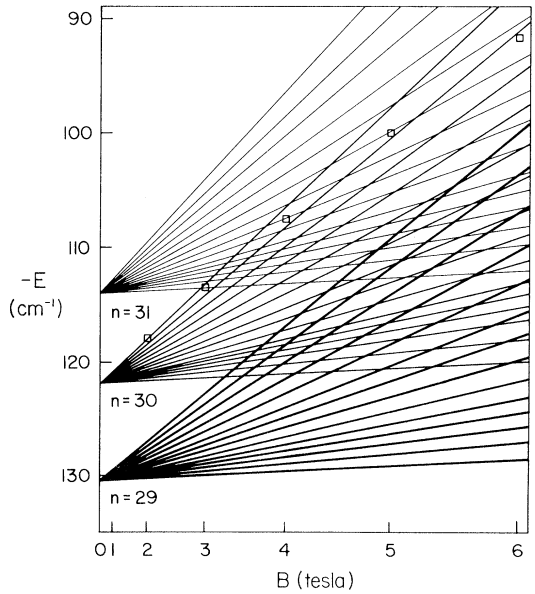

FIG. 3. The spectrum of energy levels for $m = 1$, $n = 29$, 30, and 31. The solid lines are perturbation-theory results. The points are exact semiclassical eigenvalues for the highest energy state in the $n = 30$ manifold. These were obtained by using Einstein-Brillouin-Keller quantization of numerically computed trajectories.

soning gives a complete description of the trajectories.

The exact equations of motion have been integrated numerically, and the results confirm the description given by perturbation theory.

With use of the above information about the trajectories, the spectrum of semiclassical energy levels can be calculated by quantization of action variables. I_1 and I_3 are quantized just as in the unperturbed problem,

$$I_1 = m\hbar, \quad I_3 = n\hbar. \tag{5}$$

The third quantization condition comes from the new action variable

$$A_2 = \int I_2 d\varphi_2 \tag{6a}$$

$$= (n_2 + \tfrac{1}{2})h. \tag{6b}$$

For librating trajectories, this action variable is the area inside one of the loops in Fig. 2, while for rotating trajectories it is the area under one of the corresponding curves, extended from 0 to 2π. The half-integral quantization condition (6b) is derived from a long argument that we cannot reproduce here.

A little analysis[4] now leads to the following properties of the spectrum, which are the most important results of this study.

(1) Given n and m, the total number of states is obviously $n - m$, and the first-order energy shift ΔE for every state is positive. Also in first order, ΔE is proportional to B^2.

(2) The energy shifts ΔE all lie between

$$\epsilon_0 n^2 m(5n - 2m) < \Delta E < \epsilon_0 n^2(5n^2 - 3m^2), \tag{7}$$

where $\epsilon_0 = \lambda\hbar^4/\mu^2 k^2$.

(3) There are two types of quantum states, associated with the two types of trajectory. We also call the quantum states "librational" and "rotational."

(4) Librational states are doubly degenerate. The total number of such states N_L is an even integer close to

$$N_L \simeq \frac{1}{\pi} n \cos^{-1}\left(\frac{m^2 + 3n^2/5}{m^2 - n^2}\right) - m \cos^{-1}\left(\frac{2m}{(n^2 - m^2)^{1/2}}\right). \tag{8}$$

(5) Librational levels all have energy shifts lying between the minimum given in Eq. (7) and

$$\Delta E^{\text{crit}} = \epsilon_0 (n^2/2)(n^2 + m^2). \tag{9}$$

(6) Rotational states are nondegenerate and have energy shifts which lie between ΔE^{crit} and the maximum given in (7).

(7) Energy gaps between adjacent levels are smallest for those states for which the energy shift is closest to ΔE^{crit}.

(8) Wave functions for librational levels tend to be concentrated near the $\pm z$ axes, while those for rotational levels are largest near the x-y plane.

Energy levels for $n = 30$, $m = 1$ are shown in Fig. 3. Our results are consistent with experiments and calculations done by the Massachusetts Institute of Technology group, and they provide a simple interpretation of the phenomena that are found in the spectrum.

This work was supported by research grants from the National Science Foundation, the College of William and Mary, and the U. S. Department of Energy under Contract No. W-7405-eng-26 with Union Carbide Corporation. We thank R. Hulet for providing quantum-mechanical energy calculations to compare with our results.

[a]Physics Department.

[b]Chemistry Department.

[1]L. I. Schiff and H. Snyder, Phys. Rev. 55, 59 (1939); A. F. Starace, J. Phys. B 6, 585 (1973); A. F. Starace and G. L. Webster, Phys. Rev. A 19, 1629 (1979); J. M. Wadehra, Astrophys. J. 226, 372 (1978); V. Canuto and D. C. Kelly, Astrophys. Space Sci. 17, 277 (1972); J. J. Labarthe, J. Phys. B 14, 1467 (1981); C. W. Clarke, Phys. Rev. A 24, 605 (1981); A. G. Zhilich and B. S. Monozon, Fiz. Tverd. Tela 8, 3559 (1966) [Sov. Phys. Solid State 8, 2846 (1967)]; A. R. P. Rau, Phys. Rev. A 16, 613 (1977); H. Hasegawa and R. E. Howard, J. Phys. Chem. Solids 21, 179 (1961); R. J. Elliott and R. Loudon, J. Phys. Chem. Solids 15, 196 (1960); D. R. Herrick, Phys. Rev. A 26, 323 (1982); R. Cohen, J. Lodenquai, and M. Ruderman, Phys. Rev. Lett. 25, 467 (1970); M. Ruderman, Phys. Rev. Lett. 27, 1306 (1971); E. G. Flowers, J.-F. Lee, M. A. Ruderman, P. G. Sutherland, W. Hillebrandt, and E. Müller, Astrophys. J. 215, 291 (1977); R. H. Garstang, Rep. Prog. Phys. 40, 105 (1977); J. C. Gay, in Proceedings of the NATO Advanced Study Institute on Photophysics and Photochemistry in the Vacuum Ultraviolet (to be published). An analysis quite similar to that given here, but carried out less completely, is given by E. A. Solov'ev, Pis'ma Zh. Eksp. Teor. Fiz. 34, 278 (1981) [JETP Lett. 34, 265 (1981)].

[2]M. L. Zimmerman, J. C. Castro, and D. Kleppner, Phys. Rev. Lett. 40, 1083 (1978); J. C. Castro, M. L. Zimmerman, R. G. Hulet, D. Kleppner, and R. R. Freeman, Phys. Rev. Lett. 45, 1780 (1980); D. Klepp-

ner, M. G. Littman, and M. L. Zimmerman, Sci. Am. 244, No. 5, 130 (1981).
[3]H. Goldstein, *Classical Mechanics* (Addison-Wesley, Reading, Mass., 1980), 2nd ed.
[4]J. B. Delos, S. K. Knudson, and D. W. Noid, to be published.

Stabilization of the Tearing Mode in Low-Density Tokamak Plasmas by Turbulent Electron Diffusion

E. Esarey, J. P. Freidberg, and K. Molvig
Plasma Fusion Center and Department of Nuclear Engineering, Massachusetts Institute of Technology, Cambridge, Massachusetts 02139

and

C. O. Beasley, Jr., and W. I. Van Rij
Oak Ridge National Laboratory, Oak Ridge, Tennessee 37830

(Received 24 November 1982)

The effect of turbulent electron diffusion from stochastic electron orbits on the stability of low-beta fluctuations is considered. A set of coupled self-adjoint equations is derived for the fluctuation potentials $\tilde{\phi}$ and $\tilde{A}_{\parallel}$. For the tearing mode, it is shown that stability is obtained for sufficiently large values of the diffusion coefficient. Provided $D_e \sim 1/n$, this implies that a density threshold must be surpassed before the tearing mode is observed. Numerical calculations also support this conclusion.

PACS numbers: 52.35.-g, 52.55.Gb

One of the main concerns of tokamak research is the prevention of major plasma disruptions. It is generally considered that such major disruptions must be eliminated in an actual fusion reactor to prevent prohibitive damage to the first wall. The prevailing theoretical picture of major disruptions features low poloidal mode number (low m) tearing modes which saturate to produce magnetic islands. It is possible for such magnetic islands to overlap to form large stochastic magnetic regions which enhance particle diffusion, and, in the case of major disruptions, lead to catastrophic plasma confinement loss.[1-3] Control of such disruptions requires elimination or suppression of these tearing-mode magnetic islands.

Traditionally, the tearing mode is analyzed by use of resistive magnetohydrodynamic (MHD) theory which predicts instability for $\Delta' > 0$, a condition which is generally satisfied by experimental profiles when $m = 2$. Here Δ' is the jump in the logarithmic radial derivative of the perturbed magnetic potential, $\tilde{A}_{\parallel}$, across the rational surface. Recent experimental results from Alcator C, however, show that a threshold in plasma density must be surpassed before the $m = 2$ tearing mode is observed, even though $\Delta' > 0$.[4] This observation, which is in qualitative disagreement with resistive MHD theory, motivated the present work.

In this paper, a fully kinetic approach to the tearing mode is used which includes the effects of turbulent electron diffusion resulting from stochastic electron orbits.[5] A system of coupled self-adjoint equations is derived for the perturbed potentials $\tilde{A}_{\parallel}$ and $\tilde{\phi}$. This system follows from Ampère's law and quasineutrality applied to the linear ion response and the nonlinear electron response resulting from the normal stochastic approximation (NSA).[5] The NSA includes the effects of electron diffusion in the electron response and is valid in regions where the electrons experience stochastic orbits. In this limit the NSA is essentially equivalent to the direct-interaction approximation (DIA).[6] The resulting system of coupled equations is globally valid and includes the effects of collisions, equilibrium current, diffusion, and shear. In the appropriate limit this system yields both the finite-β drift wave[7] and the tearing mode. Since the system is self-adjoint a variational principle can be formed. In this problem the tearing mode exists in a background of microturbulence such as that due to drift waves. This same set of coupled equations yields unstable finite-β drift waves when analyzed for high-m modes, from which a turbulent diffusion coeffi-

